Instability of the finite-difference split-step method applied to the nonlinear Schrödinger equation. Part II: Moving soliton

T.I. Lakoba*

Department of Mathematics and Statistics, University of Vermont, Burlington, VT 05401, USA

September 30, 2015

Abstract

We analyze a mechanism and features of a numerical instability (NI) that can be observed in simulations of moving solitons of the nonlinear Schrödinger equation (NLS). This NI is completely different than the one for the standing soliton. We explain how this seeming violation of the Galilean invariance of the NLS is caused by the finite-difference approximation of the spatial derivative. Our theory extends beyond the von Neumann analysis of numerical methods; in fact, it critically relies on the coefficients in the equation for the numerical error being spatially localized.

Keywords: operator splitting; numerical instability; nonlinear evolution equations.

*tlakoba@uvm.edu

1 Introduction

In Part I of this study [1] we analyzed a numerical instability (NI) that occurs when a soliton solution of the nonlinear Schrödinger equation (NLS)

$$iu_t - \beta u_{xx} + \gamma u|u|^2 = 0; \qquad \beta < 0 \tag{1.1}$$

is simulated by the finite-difference split-step method (FD-SSM):

(Nonlinear step):

$$\overline{u}(x) = u_n(x)\, \exp\left(i\gamma |u_n(x)|^2 \Delta t\right) \tag{1.2a}$$

(Dispersive step):

$$i\frac{u_{n+1}^m - \overline{u}^m}{\Delta t} = \frac{\beta}{2}\left(\frac{u_{n+1}^{m+1} - 2u_{n+1}^m + u_{n+1}^{m-1}}{\Delta x^{\,2}} + \frac{\overline{u}^{m+1} - 2\overline{u}^m + \overline{u}^{m-1}}{\Delta x^{\,2}}\right). \tag{1.2b}$$

Here Δt and Δx are the time and space discretization steps, $u_n^m \equiv u(x_m, n\Delta t)$, and x_m is a point in the discretized spatial domain of length L: $-L/2 < x_m < L/2$. While this FD version of the SSM is not used as widely as its spectral cousin (where the counterpart of the dispersive step (1.2b) is computed in Fourier space), it is still a well-known method (see, e.g., Refs. [8]–[15] in [1] and Ref. [2] here). Moreover, understanding a mechanism of the NI of *this* FD method for a *spatially varying* solution, such as the soliton (see Eq. (1.4) below), of a nonlinear equation may help one understand NIs of other FD methods where the standard von Neumann analysis and the method of frozen coefficients do not provide correct information.

In [1] we emphasized that the mechanism and properties of NI depend not only on the numerical method and the nonlinear equation to which it is applied, but also on the simulated solution. In fact, we showed that the NI of a *soliton* of the NLS solved by the FD-SSM is completely different from the NI of its other solution, a so-called plane wave [3]:

$$u_{\rm pw} = (A/\sqrt{\gamma})\, e^{i|A|^2 t}, \qquad A = \text{const}; \tag{1.3}$$

even when these two solutions have the same amplitude. (Earlier [4] we have demonstrated that this was also the case for the spectral SSM.) In hindsight, however, one could argue that these two NIs *should* have been different because the non-localized, constant-amplitude plane wave is quite different from the localized soliton.

In this work we show that the NI mechanisms of two "types" of solitons — standing and moving ones — are also completely different. Both these "types" are given by one formula (for $\beta < 0$):

$$u_{\rm sol}(x,t) = U_{\rm sol}(x - St)\, \exp\left[i\omega_{\rm sol} t + K_{\rm sol}(x - St)\right]; \tag{1.4a}$$

$$U_{\rm sol}(x) = A\sqrt{2/\gamma}\,\mathrm{sech}\,(Ax/\sqrt{-\beta}); \qquad \omega_{\rm sol} = A^2 + |\beta| K_{\rm sol}^2, \qquad K_{\rm sol} = S/(2|\beta|). \quad (1.4b)$$

Parameter S denotes the soliton's speed; thus the standing soliton has $S = 0$. We took the word "types" in quotes because (1.4) describes, in fact, just *one* family of solutions of the NLS, with the presence of the continuous parameter S reflecting the so-called Galilean invariance of (1.1). It is well known that *analitical* properties (such as, e.g., stability) of the soliton do *not* depend on S. Thus, one would expect their numerical (in)stabilities to also be the same or at least similar. However, as we show below, this is not the case.

This work has been motivated by the numerical results of U. Ascher [2]. He considered a collision of two solitons and observed NI for a certain relation between Δt and Δx. Since the solitons were contained inside the computational domain by periodic boundary conditions:

$$u(-L/2, t) = u(L/2, t), \qquad u_x(-L/2, t) = u_x(L/2, t), \quad (1.5)$$

simulations could be performed over a long time. At $t = 1000$, which for the parameters used in [2] corresponded to about 10 soliton collisions, a high-wavenumber *ripple occupying the entire domain* was conspicuously present in the numerical solution. However, note that a collision is a short-term event, and so just about 10 of them could not cause that slowly growing ripple. Rather, the ripple must have occurred due to NI developing for each individual (moving) soliton.

The above conclusion, while perfectly logical, was surprising to us. The reason is that by the time that we learned of Ascher's results, we had already studied [1] the NI about the *standing* soliton and knew that it developed completely differently[1] from what is described in the previous paragraph. In particular, the NI of a standing soliton does *not* cause any visible ripple outside of the soliton. We also thought that since physical properties of the soliton are independent of its speed S, as mentioned after (1.4), so should be its numerical properties. In the present study, we explain the reason behind the above "paradox". In particular, we find that the *mechanisms* of the NIs of the standing and moving solitons are completely different.

Before we proceed, a clarification is in order about what we refer to as a "moving" soliton. This is solution (1.4) *with* $S = O(1)$. Thus, we explicitly exclude the "intermediate" case of a *slowly* moving soliton, where $S \ll 1$. This case, which would provide a "bridge" between the results for the standing and moving (with $S = O(1)$) solitons, remains an unsolved problem. We briefly comment on it in Section 5 when discussing Fig. 6. On the other hand, we note that there is also an upper bound on S. Namely, we

[1] Small distortions occur at the "tails" of the soliton, which eventually, at large t, cause the soliton to start moving. This motion is eventually followed by disintegration of the pulse, but only at times that are an order of magnitude greater than those considered in [2].

showed in [5] that $K_{\rm sol} = S/(2|\beta|)$ is to be less than approximately $1/\sqrt{|\beta|\Delta t}$ in order for the FD-SSM to yield an accurate solution of the NLS (1.1).

The main part of this work is organized as follows. In Section 2 we will present a typical numerical result which demonstrates the same NI as observed by Ascher, but for different parameters (which were chosen to be closer to those used in our study of the standing soliton [1]). In Section 3 we will present a foundation on which an analysis of this NI will be built. As in [1] and earlier in [4], this foundation is an equation satisfied by *high-wavenumber* harmonics of the numerical error. We emphasize that this equation is different from its counterparts in [1] and [4] and, therefore, requires a *qualitatively* different analysis. This analysis is also different from the von Neumann analysis for a moving plane wave [6, 5] in that it *requires* one to take into account spatially dependent coefficients in the equation for the error. Our analysis is presented in Section 4. It cannot be carried out exactly, and hence we will have to approximate the soliton by a rectangular box. Such a crude approximation cannot be expected to yield accurate predictions about the NI's threshold, spectral location, and growth rate. However, it still reveals the mechanism of this NI. Moreover, it explains qualitatively, and sometimes even quantitatively, a number of the NI's features. These features are listed and explained in Section 5. In Section 6 we summarize our conclusions and also explain why the NI observed for the standing soliton [1] is not observed for the moving one.

2 Numerical experiment

The initial condition in our numerical simulations was

$$u_0(x) = \operatorname{sech}(x)\, e^{iK_{\rm sol}x} + \xi, \tag{2.1}$$

where ξ is a Gaussian noise with amplitude of order 10^{-10} and $K_{\rm sol}$ is related to the soliton's speed in (1.4) by $S = 2K_{\rm sol}|\beta|$. The result reported below is for $S = 1.885$, which was chosen near $S = 2$ and so as to make the exponential factor in (2.1) be exactly periodic in the computational domain. Thus, periodic boundary conditions (1.5) were used in all our simulations[2]. Other computational parameters were: $L = 40$, $N = 2^{10}$, $t = 1500$. Parameters of the NLS were: $\beta = -1$ and $\gamma = 2$. As in [1], we will see that a key quantity in the analysis will be

$$C = (\Delta t/\Delta x)^2\,; \tag{2.2}$$

[2]For the standing soliton in a sufficiently large domain, considered in [1], any type of boundary conditions could be used without affecting the soliton, and this also would not affect properties of the NI. In contrast, for the moving soliton, periodic boundary conditions are the only ones that can support such a solution of (1.1) over an arbitrarily long time.

so we will refer to it rather than to the time step Δt alone.

Panels (a) and (b) of Fig. 1 display a typical spectrum of the numerical solution and an envelope of the unstable mode, obtained for the above parameters and for $C = 0.9$. This value for C was chosen to contrast the cases of moving and standing solitons: In [1] we showed that the NI threshold for the standing soliton with the same amplitude as in (2.1) was just slightly above $C = 1$. Thus, NI of a moving soliton sets in for smaller C values (or, equivalently, time steps) than the NI of the standing soliton. In fact, we have observed (a weak) NI of the moving soliton with the same parameters for C as small as 0.5. Let us note that the amplitude of the greatest of unstable modes in Fig. 1(a) is about six orders of magnitude smaller than the soliton. As this mode continues to grow, it becomes visible on the linear scale and in the x-space is observed as a high-frequency ripple: see Fig. 7(b) in [2].

Panels (a) and (c) of Fig. 1 illustrate an important difference between the NIs of the moving and standing solitons. Namely, the bandwidth of the unstable modes in Fig. 1(a) (see also Fig. 7(b) below) is considerably narrower than that in Fig. 1(c). This is one of the factors that lead to different equations for the numerical error for the moving and standing solitons, as we will explain in the next section. Let us also clarify that the plateaus near $k = \pm k_{\max}$ in Fig. 1(c) are *not* the result of a merger of peaks like those seen in Fig. 1(a) at a later stage of their evolution. (Such a merger could have occurred via broadening of the peaks due to four-wave mixing.) The plateaus of unstable harmonics of the standing soliton develop right away and preserve their shape during the evolution.

3 Derivation of equation for numerical error

In order to make this paper self-contained, we present all steps of this derivation, even though some of them were originally presented in [1]. We will note those steps where differences from the case of the standing soliton occur.

In view of periodic boundary conditions (1.5), the dispersive step of the FD-SSM (1.2) can be written as

$$u_{n+1}(x) = \mathcal{F}^{-1}\left[e^{iP(k)}\,\mathcal{F}\left[\overline{u}(x)\right]\right], \tag{3.1}$$

where

$$e^{iP(k)} \equiv \frac{1 + 2i\beta r \sin^2(k\Delta x/2)}{1 - 2i\beta r \sin^2(k\Delta x/2)} = \exp\left[2i \arctan\big(2\beta r \sin^2(k\Delta x/2)\big)\right], \qquad r = \frac{\Delta t}{\Delta x^2}, \tag{3.2}$$

$\overline{u}$ is defined in (1.2a), and $\mathcal{F}$, $\mathcal{F}^{-1}$ are the discrete Fourier transform and its inverse. Equations (1.2a), (3.1), and (3.2) are the effective equations of the FD-SSM. Their

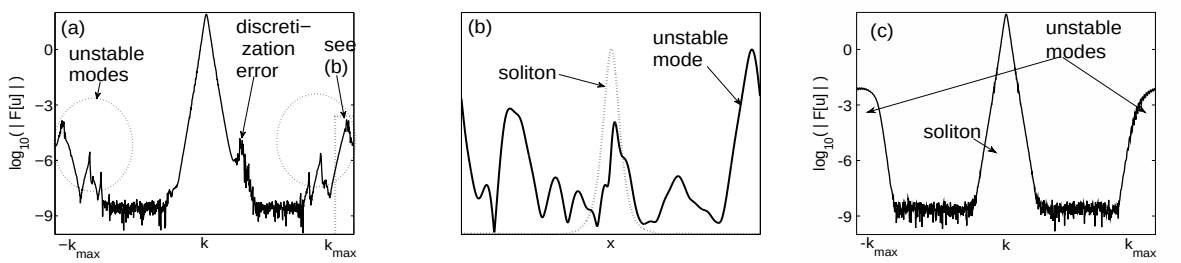

Figure 1: (a) Logarithm of the Fourier spectrum of the numerical solution described in the text. Unstable modes are circled at both ends of the k-domain. The discretization error seen on the right of the soliton is due to the approximation of the u_{xx}-term in (1.1) by the finite-difference method (1.2b). It develops for $t = O(1)$ and only insignificantly change its size at later times. (b) The envelope of the unstable mode filtered out by a band-pass filter shown near the right edge of (a). It has an irregular shape, which changes with time, because it is a packet of *several* plane waves. The soliton is shown by the dotted line. Both the soliton and the unstable mode are normalized to have the same amplitude. (c) Logarithm of a typical spectrum of a numerically unstable solution of (1.1) with the background being a *standing* soliton.

solution is sought in the form

$$u_n = u_{\rm b} + \tilde{u}_n, \qquad |\tilde{u}_n| \ll |u_{\rm b}|, \tag{3.3}$$

where $u_{\rm b}$ is the background solution and $\tilde{u}_n$ is the numerical error. Below we take $u_{\rm b}$ to be the moving soliton (1.4). Substituting (3.3) into (3.1) and linearizing, one obtains the general equation for the error:

$$\mathcal{F}\left[\tilde{u}_{n+1}\right] = e^{iP(k)}\mathcal{F}\left[e^{i\gamma|u_{\rm b}|^2\Delta t}\big(\tilde{u}_n + i\gamma\Delta t(u_{\rm b}^2\tilde{u}_n^* + |u_{\rm b}|^2\tilde{u}_n)\,\big)\,\right]. \tag{3.4}$$

Using the fact that we are specifically considering only those Fourier harmonics of $\tilde{u}_n$ that can potentially become numerically unstable, we will simplify (3.4) to a form amenable to analysis.

The exponential growth of $\tilde{u}_n$ can occur only if there is sufficiently strong coupling between $\tilde{u}_n$ and $\tilde{u}_n^*$ in (3.4). This coupling is the strongest when the temporal rate of change of the relative phase between those two terms is minimized. In [4] we showed that this rate can be small only for those k where the exponent $P(k)$ is close to a multiple of π. Using (3.2) (see also Fig. 2), we see that this can occur only for sufficiently high k where $\sin^2(k\Delta x/2) = O(1)$ rather than $O(\Delta x^{\,2})$. This is confirmed by the numerical experiment in Section 2: see Fig. 1(a).

When (3.3) is substituted into (3.4), the next step is to expand the phase $P(k)$. In so doing, we use the fact that $r \gg 1$, because

$$r = \Delta t/\Delta x^{\,2} = C/\Delta t \gg 1, \tag{3.5}$$

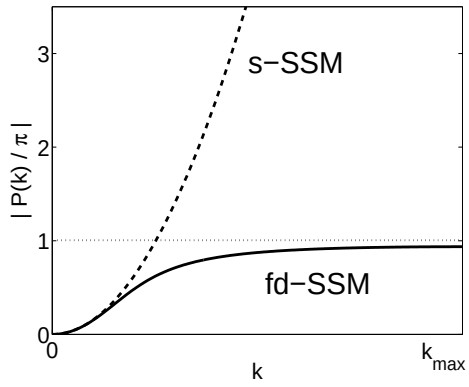

Figure 2: Normalized phase: $|\beta|k^2\Delta t$ for the spectral (s-) SSM (dashed) and as given by (3.2) for the FD-SSM (solid). In both cases, $r = 5$. The horizontal line indicates the condition of the first resonance: $|P(k)| = \pi$.

and from Section 2 we know that NI is observed when $C = O(1)$. Then, expanding the exponent in (3.2) in powers of $(1/r)$, we find:

$$-P(k) = \pi - \frac{1}{|\beta| r \sin^2(k\Delta x/2)} + O\left(\frac{1}{r^3}\right). \tag{3.6}$$

It is in (3.6) that the main difference between the present derivation and the one for the standing soliton [1] occurs. In [1] we proceeded to expand the second term on the right-hand side (r.h.s.) using the numerical observation (see Fig. 1(c)) that the highest unstable harmonic is at $k_{\max}$ and that the bandwidth of unstable modes satisfies $|k - k_{\max}| \gg 1$, where $k_{\max} = \pi/\Delta x$. However, for the moving soliton, bandwidth of unstable modes is found to be of order one; note that they are seen as peaks in Fig. 1(a) and 7(b) rather than as a plateau in Fig. 1(c). From Fig. 1(a) one can also see that the spectrum of unstable modes is approximately symmetric relative to some value $k = O(1)$. It is, therefore, convenient to seek

$$\tilde{u}_n = e^{i\omega_{\rm sol} t_n + iK_{\rm sol}(x - St_n)} \left(p_n(x) e^{iK_0 x} + q_n^*(x) e^{-iK_0 x} \right). \tag{3.7}$$

Here $K_0 = O(k_{\max}) \gg 1$, which remains to be determined, and $p_n(x)$, $q_n(x)$ may vary with x on a scale of order one[3]. Then, $(\pm K_0 + K_{\rm sol})$ are the approximate locations of the unstable peaks. With this observation and using (3.5), Eq. (3.6) is reduced to

$$-P(k) = \pi - \frac{\Delta t}{C|\beta| \sin^2(K_0 \Delta x/2)} + O\left(\Delta t^2\right), \tag{3.8}$$

[3]This is because the spectral width of the peaks of unstable modes is of order one, and so is the product of the spectral and spatial widths for any signal.

where we have also used $K_{\rm sol} = O(1)$ (see Introduction) and $\Delta x = O(\Delta t)$. Thus, the bandwidth of the unstable peaks does not explicitly enter into our analysis; rather, it will be determined later from those values of K_0 for which unstable modes can exist.

The next few steps are similar to those in [1] and so we present them briefly. Introducing a new variable

$$\tilde{v}_n = \left(e^{-i\pi}\right)^n \tilde{u}_n = (-1)^n \tilde{u}_n, \tag{3.9}$$

and substituting (3.8) (with term $O(\Delta t^2)$ being omitted) into (3.4) one obtains:

$$\mathcal{F}[\tilde{v}_{n+1}] = \exp\left(-\frac{i\Delta t}{C\beta \sin^2(K_0\Delta x/2)}\right) \mathcal{F}\left[e^{i\gamma|u_{\rm b}|^2\Delta t}\left\{\tilde{v}_n + i\gamma\Delta t(u_{\rm b}^2\tilde{v}_n^* + |u_{\rm b}|^2\tilde{v}_n)\right\}\right]. \tag{3.10}$$

Note that (3.10) describes a *small* change of $\tilde{v}_n$ occurring over the step Δt, because for $\Delta t \to 0$, the r.h.s. of that equation reduces to $\mathcal{F}[\tilde{v}_n]$. Therefore we can approximate the *difference* equation (3.10) by a *differential* equation, as explained in [1]. In the leading order, the result is:

$$i\tilde{v}_t + \tilde{v}/(C|\beta|\sin^2(K_0\Delta x/2)) + \gamma(u_{\rm b}^2\tilde{v}^* + 2|u_{\rm b}|^2\tilde{v}) = 0; \tag{3.11}$$

recall that $\beta < 0$. Its apparent difference from the counterpart for the standing soliton — Eq. (3.14) in [1] — is in the absence of the $\tilde{v}_{xx}$-term. The reason behind that difference is explained after Eq. (3.6) above.

Finally, using (3.7) and (1.4), separating the e^{iK_0x} and e^{-iK_0x} terms, and employing the change of variables $(x,t) \longrightarrow (z = x - St, t)$, we obtain:

$$p_t - Sp_z = i\mu p + i\gamma U_{\rm sol}^2(z)\,(2p+q), \tag{3.12a}$$

$$q_t - Sq_z = -i\mu q - i\gamma U_{\rm sol}^2(z)\,(p+2q), \tag{3.12b}$$

where $\{p(x,t),\, q(x,t)\}$ are time-continuous counterparts of $\{p_n(x),\, q_n(x)\}$ and

$$\mu = \frac{1}{C|\beta|\sin^2(K_0\Delta x/2)} - A^2 + |\beta|K_{\rm sol}^2. \tag{3.13}$$

Similarly to [1], one can show that boundary conditions for Eqs. (3.12) are periodic. To be more precise, in light of (3.7) it is $p(x,t)\exp[i(K_{\rm sol}+K_0)x]$ and $q(x,t)\exp[i(K_{\rm sol}-K_0)x]$ that are to be spatially periodic. However, in all our numerical simulations we have used the initial condition where $K_{\rm sol}$ was on the spectral grid (see, e.g., Section 2), whence $\exp[iK_{\rm sol}x]$ is periodic. As for the yet unknown K_0, when later on we determine a range for its values, we will select from that range only the values on the spectral grid; hence $\exp[\pm iK_0x]$ will be periodic. Thus, without loss of generality, we require

$$p(-L/2,t) = p(L/2,t), \qquad p_x(-L/2,t) = p_x(L/2,t), \tag{3.14}$$

and similarly for q. Since these conditions hold at all times t, the first argument of p and q in (3.14) may equally be interpreted as either x or z.

In the next Section we will use Eqs. (3.12)–(3.14) to study the NI of a moving soliton. As we have noted already, they differ from their counterpart for the standing soliton in that the terms with the second-order spatial derivative are absent. This is a direct consequence of the numerically observed width of the unstable peaks being of order one for the case of moving soliton (Fig. 1(a)), whereas such peaks (or, rather, a plateau) are considerably wider in the Fourier space for the standing soliton (Fig. 1(c)). We also note that this difference is an "external" piece of information in the sense that it is supplied to the analysis by the numerics. Determination *from purely analytic considerations* of how the speed of the soliton affects the aforementioned features of unstable modes in Fourier space remains an open problem.

However, the *main difference* of Eqs. (3.12)–(3.14) from their counterparts for the standing soliton is the $S\partial_z$-terms, which were absent for the standing soliton. These terms represent convection rather than dispersion; in other words, they account for the modes' *passing through* the soliton (in the reference frame where the soliton is not moving). We will show that it is this *relative motion* of the soliton and certain high-k Fourier harmonics that may cause NI. In contrast, NI of a standing soliton was shown [1] to be caused by modes that do not move relative to the soliton.

4 Analysis of NI based on equations for numerical error

Let us describe challenges in using Eqs. (3.12)–(3.14) to study NI of a moving soliton. Most obviously, they have a spatially varying coefficient $U_{\rm sol}^2(z)$. Hence, in a standard way, one would expect to relate them to an eigenvalue problem which, in turn, would have to be solved numerically, as in [1]. However, unlike in [1], one of the parameters, μ, depends on an *unknown* value of K_0, related to the spectral location of unstable peaks, and this makes the eigenvalue-based approach impractical. Indeed, if one seeks a solution of (3.12) in the standard form $(p(z,t),\, q(z,t))^T = \vec{\rho}(z)e^{\lambda t}$, one obtains an eigenvalue problem

$$\left(iS\sigma_3\partial_z - \mu - \gamma U_{\rm sol}^2(z) \begin{pmatrix} 2 & 1 \\ 1 & 2 \end{pmatrix} \right) \vec{\rho} = i\lambda\sigma_3\vec{\rho}, \tag{4.1}$$

with $\vec{\rho}$ satisfying periodic boundary conditions (see (3.14)); here $\sigma_3 = \mathrm{diag}(1,-1)$ is a Pauli matrix. Given parameters of the soliton, the NLS, and the numerical scheme (i.e., C), one knows all coefficients in (4.1) except K_0 and the eigenvalue λ. Then, finding λ corresponding to NI in the problem would require scanning through many values of

K_0 to determine those special ones where a NI exists. Not only would this make the numerical solution of (4.1) considerably more time-consuming than its counterpart for the standing soliton, but it would also not provide any insight into *why* the instability occurs only for some special values of K_0 but not for all K_0. Such an insight could only come from an analytical solution of (4.1). Since we have been unable to find such a solution exactly, we had to resort to an approximation.

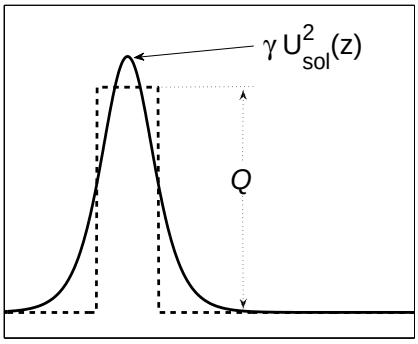

Figure 3: Schematics of a box profile approximating $\gamma U_{\rm sol}^2$ in (3.12).

A widely used approximation consists of replacing $\gamma U_{\rm sol}^2(z)$ with a box profile of width ℓ and height Q, as illustrated in Fig. 3. While such a crude approximation cannot be expected to yield a quantitatively accurate description of NI, it still allows us to understand the nature of unstable modes as well as the dependence of NI's features on such parameters as $K_{\rm sol}$ (or, equivalently, S), the length of the spatial domain L, and the mesh size Δx.

Without loss generality the left-hand edge of the box can be put at $z = 0$. Then the solutions of (4.1) with $U_{\rm sol}^2$ replaced by the box profile are given by the following expressions inside and outside the box:

$$0 \le z \le \ell:$$
$$\vec{\rho} = a_{\rm in}^- \begin{pmatrix} \mu+\eta+2Q \\ -Q \end{pmatrix} e^{i\kappa_{\rm in}^- z} + a_{\rm in}^+ \begin{pmatrix} -Q \\ \mu+\eta+2Q \end{pmatrix} e^{i\kappa_{\rm in}^+ z}, \tag{4.2a}$$

$$\ell \le z \le L:$$
$$\vec{\rho} = a_{\rm out}^- \begin{pmatrix} 1 \\ 0 \end{pmatrix} e^{i\kappa_{\rm out}^- z} + a_{\rm out}^+ \begin{pmatrix} 0 \\ 1 \end{pmatrix} e^{i\kappa_{\rm out}^+ z}, \tag{4.2b}$$

where

$$\eta = \sqrt{(\mu+2Q)^2 - Q^2}, \qquad \kappa_{\rm in}^{\pm} = (-i\lambda \pm \eta)/S, \qquad \kappa_{\rm out}^{\pm} = (-i\lambda \pm \mu)/S. \tag{4.3}$$

The constants $a^{\pm}_{\text{in, out}}$ are found using the continuity of this solution at $z = \ell - 0$ and $z = \ell + 0$ and at $z = L$ and $z = 0$, with the latter condition being equivalent to the periodic boundary condition. The existence of nontrivial solutions of the resulting linear system determines the eigenvalue λ:

$$e^{\lambda L/S} = R \pm \sqrt{R^2 - 1}, \tag{4.4a}$$

$$R = \cos\Phi_+ + \frac{Q^2}{(\mu + \eta + 2Q)^2 - Q^2} \left(\cos\Phi_+ - \cos\Phi_-\right). \tag{4.4b}$$

$$\Phi_\pm = (\mu(L - \ell) \pm \eta\ell)/S \tag{4.4c}$$

Eigenvalues with $\text{Re}\lambda > 0$ exist for

$$|R| > 1. \tag{4.5}$$

Thus, (4.5) along with (4.4b,c) is the condition of NI of a moving soliton.

Let us now point out the two main differences between the analyses of the NI for a moving soliton (in this Section) and a standing one (in [1]). First, the box-profile approximation of the soliton cannot be used to find unstable modes of the standing soliton, because those modes can exist *only* on the soliton's "tails", which have finite slope. More specifically, they can exist only due to a balance between the potential created by the soliton and the dispersion due to a ∂_{zz}-like term. Thus, they cannot be supported by the discontinuous "jumps" on the box's sides. In contrast, unstable modes of a moving soliton are supported by some sort of resonance that occurs due to periodic passage (governed by the convective terms $S\partial_z$ in (3.12)) of Fourier harmonics through the soliton; see next paragraph.

Second, the analysis for a moving soliton critically depends on the soliton's speed, S, not being zero (note the S in the denominators in (4.3) and (4.4)). Physically, this means that high-k harmonics, for which (3.11) and (3.12) were derived, move with speed S relative to the soliton. This is because these harmonics have a vanishingly small group velocity, $(dP(k)/dk)/\Delta t$ (see Fig. 2) in the original reference frame where the soliton is moving with speed S. Thus, the possibility of the NI *inherently* depends on this relative motion. In contrast, unstable modes of a standing soliton do not move relative to it.

5 Features of NI of moving soliton and their explanation

As we announced in Introduction, the focus of our study is to understand a mechanism of the NI of a moving soliton. This includes finding modes that cause NI, as well as

estimation of their growth rate and a threshold for their appearance. Numerical results of [2] and Section 2 presented evidence, and the analysis of Section 4 confirmed, that these unstable modes are delocalized, plane-wave-like packets. The NI is caused by a pair of these waves, denoted as p and q in Section 4, repeatedly (due to the periodic boundary conditions) passing through the soliton and interacting with each other. This situation should be contrasted with the unstable modes of a standing soliton [1], which are localized and "pinned" at the "tails" of its host pulse.

Below we will show how to use Eqs. (4.4), (4.5) to explain qualitatively, and sometimes even quantitatively, a number of features (including the growth rate) of the NI of a moving soliton, observed in numerical simulations. A list of these features follows in the next paragraph. The NI threshold $\Delta t_{\rm thresh}$ and its dependence on Δx will be discussed in Section 6.

(i) The height and spectral width of unstable peaks decrease as their wavenumber $|k|$ decreases;

(ii) The wavenumbers of the unstable peaks vary in inverse proportion to Δx;

(iii) The wavenumbers of the peaks are *not* symmetric about $K_{\rm sol}$, as one could have concluded from (3.7);

(iv) The instability growth rate, $\mathrm{Re}\lambda$, varies in inverse proportion to the length L of the computational domain;

(v) The instability decreases as C is decreased or as $K_{\rm sol}$ is increased.

(vi) The unstable mode could stay "hidden" and then appear above the noise floor only after some time, which for sufficiently small C can be on the order of hundreds of units.

Feature (i) is illustrated by Fig. 1(a), while evidence for the other features will be given as we proceed.

A convenient way to analyze the NI condition is to consider a parametric representation $R = R(\mu)$ and $K_0 = K_0(\mu)$, where for the latter one inverts (3.13):

$$K_0 = \frac{2}{\Delta x}\arcsin\sqrt{\frac{1}{C|\beta|(\mu - |\beta|K_{\rm sol}^2 + A^2)}}. \tag{5.1}$$

The resulting plot of $|R|$ versus K_0 is shown in Fig. 4(a) for the same parameters as used for Fig. 1(a,b). For other parameters, the plot $R = R(K_0)$ looks qualitatively similar. We have also used the values

$$\ell = 1.76, \qquad Q = 4/\ell, \tag{5.2}$$

where the first is the full width at half maximum of the sech^2 profile and the second follows from $Q\ell = \int_{-\infty}^{\infty} \gamma U_{\rm sol}^2(z)dz = 4$ for $A = |\beta| = 1$. In Fig. 4(b) we show a detailed view of (a) that demonstrates that the NI condition (4.5) is satisfied only in narrow bands of wavenumbers k. As we noted before (3.14), values of K_0 must be on the spectral grid, and hence the increasingly narrow bands where $|R| > 1$ occurring towards the decreasing values of K_0 may simply miss points on the spectral grid. This, along with the fact that the "tips" of $|R|$ that exceed 1 become smaller as K_0 decreases explains *feature (i)* stated above.

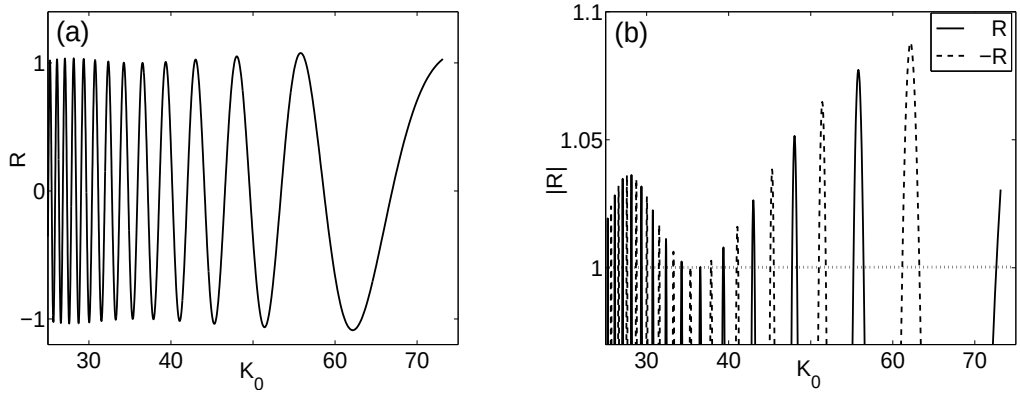

Figure 4: (a) $R(K_0)$ and (b) a detailed view of (a) near $\pm R(K_0) = 1$.

Feature (ii) is illustrated by Table 1. The simulation parameters are the same as those used for Fig. 1, except that we have varied C and also compared the cases of $N = 2^{10}$ and $N = 2^{11}$ grid points, so that the corresponding Δx differ by a factor of 2. The locations of the respective peaks of unstable modes is seen to differ by an approximately reciprocal factor. An explanation for this follows directly from (5.1).

Results of Table 1 also illustrate *feature (iii)*: the positive and their respective negative peaks are not symmetric about $K_{\rm sol}$. That is,

$$(k_{\rm peak}^{+} + k_{\rm peak}^{-})/2 \neq K_{\rm sol}. \tag{5.3}$$

The l.h.s. of this formula is plotted in Fig. 5(a). The analytical estimate for this quantity is obtained as follows. Since at any given time the soliton occupies only a small part of the computational domain, the unstable mode is described for the most part by its "outside of the box" expression (4.2b). Along with the expression (4.3) for $\kappa_{\rm out}^{\pm}$ and the fact that for the unstable modes λ is purely real (see (4.4a) and (4.5)) this implies that $\{p,\, q^*\} \propto \exp[-i(\mu/S)z]$. Then from (3.7) it follows that

$$k_{\rm peak}^{\pm} = \pm K_0 + K_{\rm sol} - \mu/S, \tag{5.4}$$

C	$k^{\pm}_{\rm peak}$, $N = 2^{10}$			$k^{\pm}_{\rm peak}$, $N = 2^{11}$		
0.9	77.0	62.5	56.2	154.4	125.0	112.2
	−76.2	−61.8	−55.6	−153.3	−124.4	−111.7
1.0	63.9	56.4	51.5	128.0	112.6	102.9
	−63.1	−55.7	−50.9	−127.2	−112.0	−102.4
1.25	71.8	58.7	52.0	144.5	117.2	103.8
	−70.7	−57.8	−51.2	−143.4	−116.2	−103.0
1.50	74.0	57.6	50.5	149.5	115.3	100.7
	−72.8	−56.6	−49.5	−147.7	−114.2	−99.7

Table 1: Wavenumbers of the three most unstable peaks; $k^+ > 0$, $k^- < 0$. For $C \geq 1$ the outer peaks (those with larger $|k^{\pm}_{\rm peak}|$) contain several grid points; only the wavenumber of the maximum $|\mathcal{F}[u](k)|$ is listed in those cases.

which confirms (5.3).

Figure 5 demonstrates that the locations of unstable peaks are quite accurately predicted by our approximate analysis. However, this analysis considerably (by a factor of order two for $C \approx 1$) overestimates the instability growth rate. Moreover, as C decreases, the discrepancy between the analytical and numerically observed growth rates increases.

Yet, our analysis easily explains *feature (iv)*, whereby the instability growth rate scales in inverse proportion to the length of the computational domain (assuming that it far exceeds the width of the soliton). To that end, we will first explain why one typically has

$$|R| - 1 \ll 1 \qquad \text{where } |R| > 1, \tag{5.5}$$

as seen in Fig. 4. For C, A, $K_{\rm sol}$ all of order one, μ is also of order one; see (3.13). (For the specific values $A = K_{\rm sol} = |\beta| = 1$ used here, $\mu \geq 1/C$.) Then, even if we conservatively assume $\mu > 0$, then from (4.3) one has $\eta/Q > \sqrt{3}$, and then

$$(\mu + \eta + 2Q)^2/Q^2 > (\sqrt{3} + 2)^2 \approx 14. \tag{5.6}$$

We stress that this is a conservatively low estimate; in our simulations the respective values were higher than about 22. Relation (5.6) implies that the second term in (4.4b) is small. From this one concludes that the "bumps" of $|R|$ occur where $\Phi^+ \approx \pi n$ for some integer n and that

$$|R| - 1 \leq 2/\left(\left((\mu + \eta)/Q + 2\right)^2 - 1\right), \tag{5.7a}$$

which in view of (5.6) and the note below it we regard as as small number. Combining

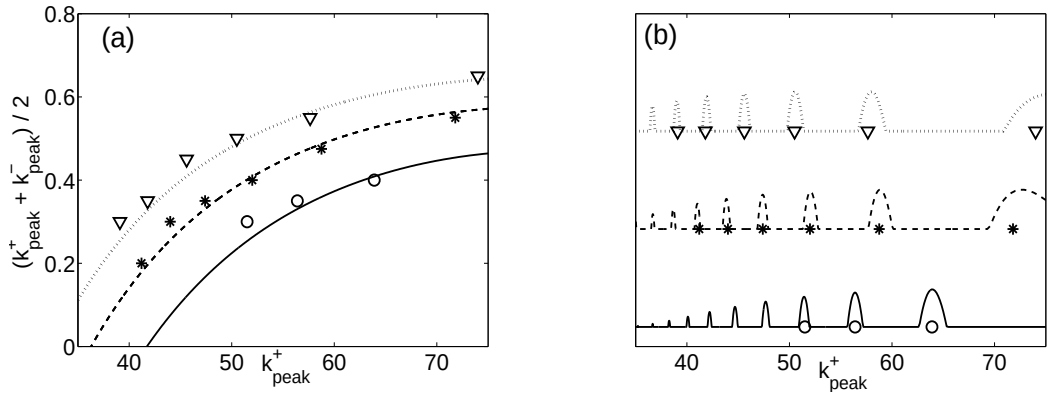

Figure 5: (a) The l.h.s. of (5.3) versus the wavenumber of unstable peaks with $k > 0$. Solid, dashed, and dotted lines are the analytical expressions obtained from (5.4) for $C = 1$, 1.25, 1.5 and the parameters stated in the text. Circles, stars, and triangles are the respective numerical values. (b) Line and symbol styles pertain to the same cases as in (a). Lines are obtained from the analytical expressions for $\max(|R|, 1)$, so that the "bumps" indicate locations of bands of unstable modes. Symbols indicate the locations of numerically obtained unstable peaks. The data for different values of C are vertically shifted for clarity.

this with (4.4a) one obtains

$$\lambda \approx \sqrt{2}(S/L)\sqrt{|R| - 1}, \tag{5.7b}$$

which provides the reason behind feature (iv).

Formulas (5.7) and (3.13) also explain why increasing $K_{\rm sol}$ (and hence $S = 2|\beta|K_{\rm sol}$) *eventually* reduces the growth rate of the NI; this was stated as part of *feature (v)*. Below we will present our argument as a crude estimate but will confirm it with analytical expressions following from our analysis above and also by results of numerical simulations. For the purpose of this estimate we will assume that the first two terms on the r.h.s. of (3.13) approximately cancel each other, and then $\mu \sim K_{\rm sol}^2$. With the same accuracy, from (4.3) we have $\eta \sim K_{\rm sol}^2 + 2Q$, and then from (5.7) we find

$$\max \lambda \propto K_{\rm sol}/(K_{\rm sol}^2/Q + 2). \tag{5.8}$$

This shows that as $K_{\rm sol}$ increases, the instability growth rate eventually vanishes, although it does grow initially as $K_{\rm sol}$ increases from zero. These conclusions are qualitatively confirmed by Fig. 6. As an aside, let us note that the broad "pedestals" of the unstable peaks for $K_{\rm sol} = 0.3$ and 0.5 seen in Fig. 6(b) are reminiscent of the spectrally

broad plateau of unstable modes for the case of a standing soliton in Fig. 1(c). This agrees with our remark at the end of Introduction that for sufficiently small $K_{\rm sol}$ (or S) there should be a regime where the NI of a moving soliton turns into that of a standing soliton. Our analysis cannot capture this regime for the following reason. For a standing soliton, unstable modes *fundamentally* require the existence of the soliton's "tails", by which those modes are supported. The box-like approximation of the soliton used above does not have "tails". Therefore, bridging the analyses in the cases of a pulse with and without "tails" remains an open problem.

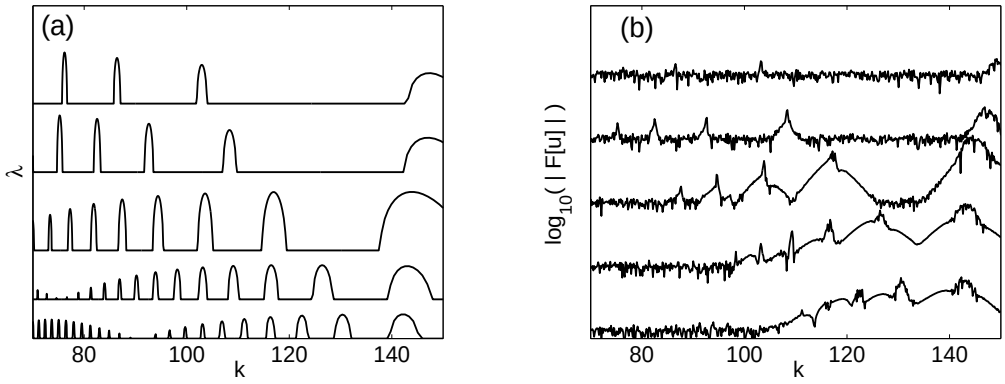

Figure 6: (a) NI growth rate, computed from (5.7), as a function of wavenumber. The parameters are as previously described in the text, except that $C = 1.25$, $K_{\rm sol}$ is varied as stated below, and $N = 2^{11}$. (This larger N, leading to a smaller Δx, is needed to keep the discretization error due to the FD approximation (1.2b) sufficiently small for the larger values of $K_{\rm sol}$.) The curves, from bottom to top, correspond to $K_{\rm sol} =$ 0.31, 0.47, 0.94, 1.57, 2.04; they are vertically shifted for clarity. Note that only the higher-k part of the spectrum is shown. (b) The results of numerical simulations for the same respective parameters as in (a).

The other part of *feature (v)* — that as C decreases, the NI growth rate decreases — is explained similarly to the above. Indeed, it follows from (3.13) that μ increases as C decreases, which via (5.7) implies that λ decreases. The main difference from (5.8) here is that this decrease occurs monotonically with C.

Finally, *feature (vi)*, which can be referred to as "delayed" NI, is illustrated by Fig. 7(a). This seemingly mysterious feature has a simple explanation. The noise $\xi(x)$ in the initial condition, (2.1), consists of Fourier harmonics with random phases and random amplitudes. Growth of any Fourier harmonic occurs only as long as it overlaps with the unstable mode. Examples of spectral and spatial profiles of the unstable mode

are shown in Fig. 7(b,c). The overlap factor between a Fourier harmonic and this mode,

$$\mathrm{OF}(k) = \left| \int_{-L/2}^{L/2} e^{-ikx} u_{\mathrm{mode}} dx \right| \Big/ \sqrt{L \int_{-L/2}^{L/2} |u_{\mathrm{mode}}|^2 dx}, \tag{5.9}$$

is shown in Fig. 7(d). A point to note is that for all wavenumbers including the location of the spectral peak of the unstable mode, k_{peak}, this factor is considerably (see below) less than one:

$$|\mathrm{OF}(k)| \le |\mathrm{OF}(k_{\mathrm{peak}})| \approx 0.7. \tag{5.10}$$

Let us consider evolution of the Fourier harmonic with $k = k_{\mathrm{peak}}$:

$$\mathcal{F}[u](k_{\mathrm{peak}}, t) = \mathcal{F}[u](k_{\mathrm{peak}}, 0) \left(\mathrm{OF}(k_{\mathrm{peak}})\, e^{\lambda_{\mathrm{most}} t} + \sum_j \mathrm{OF}(k_j) e^{\lambda_j t} \right), \tag{5.11a}$$

where λ_{most} and λ_j are the eigenvalues of the most unstable mode and all other modes, respectively. Over long time, the second term on the r.h.s. of (5.11a) is negligible compared to the first one. Therefore, asymptotically,

$$\mathcal{F}[u](k_{\mathrm{peak}}, t) \approx \mathrm{OF}(k_{\mathrm{peak}})\, \mathcal{F}[u](k_{\mathrm{peak}}, 0) e^{\lambda_{\mathrm{most}} t}. \tag{5.11b}$$

Thus, the spectral peak of the most unstable mode will become visible above the noise floor, $\mathcal{F}[u](k)_{\mathrm{floor}}$, when

$$\left| \mathrm{OF}(k_{\mathrm{peak}})\, \mathcal{F}[u](k_{\mathrm{peak}}, 0)\, e^{\lambda_{\mathrm{most}} t} \right| > \mathcal{F}[u](k)_{\mathrm{floor}}. \tag{5.12a}$$

Note that $\mathcal{F}[u](k)_{\mathrm{floor}}$, which is estimated from the spectrum by simple visual inspection, is determined not by the average values of the magnitudes of Fourier harmonics, but by their top values: just examine any plot of Fourier spectra in this paper. From (5.12a), one has:

$$t_{\mathrm{delay}} \approx \left(\ln\left[1/\mathrm{OF}(k_{\mathrm{peak}})\right] + \ln\left[\mathcal{F}[u](k)_{\mathrm{floor}} / \mathcal{F}[u](k_{\mathrm{peak}}, 0)\right] \right) / \ \mathrm{Re}\lambda_{\mathrm{most}} \approx \left(0.35 + (\gtrsim 0)\right) / \mathrm{Re}\lambda_{\mathrm{most}}, \tag{5.12b}$$

where in the last step we used (5.10) and the note after (5.12a). One can see that the weaker the NI (i.e., the smaller C and hence $\mathrm{Re}\lambda_{\mathrm{most}}$), the longer it takes the NI to become observable. The dependence of the delay time on the initial noise realization, illustrated in Fig. 7(a), is also evident from (5.12b).

6 Conclusions and discussion

In this work we have analyzed the NI that may occur when a moving soliton (with speed $S = O(1)$) is simulated by the FD-SSM. As in our earlier papers [4, 1], the analysis

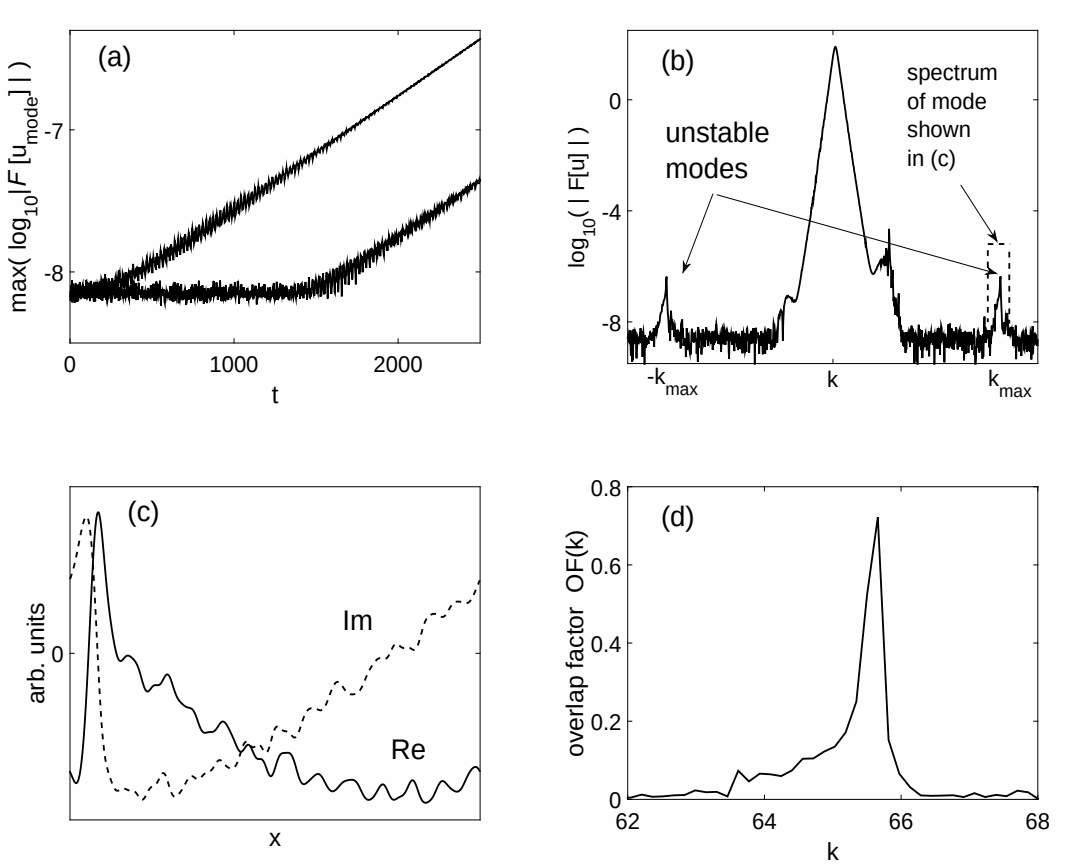

Figure 7: Simulation parameters are the same as in Section 2, except that $C = 0.7$ and $t = 2500$. (a) Evolution of the height of the right spectral peak (see (b)) of the unstable mode for two different noise realizations in initial condition (2.1). (b) Fourier spectrum of the numerical solution corresponding to the smaller delay time in (a). (c) Real and imaginary parts of the envelope, $\exp[-ik_{\rm peak}x]\, u_{\rm mode}$, of the mode indicated in (b). (d) Overlap factor computed from (5.9).

went beyond the standard von Neumann analysis of numerical methods. In fact, in our analyses it was *critical* to account for the fact that the background solution had spatially varying profile (more specifically, it was localized).

The moving and standing solitons are members of the same family of solutions, (1.4), where the soliton's speed enters as a continuous parameter. It is well known

that analytical properties of the soliton do not depend on S. Yet, the NIs of these two "types" of solution were numerically shown to manifest themselves completely differently [1, 2]. Namely, while the unstable modes of a standing soliton are localized at the soliton's "tails", unstable modes of a moving soliton are plane waves occupying the entire computational domain. The NI is caused by interaction of two spectrally well-separated waves, denoted as p and q in (3.7), at the location of the soliton.

Our findings support the statement that we announced in Part I of this study [1] and also in Introduction: Mechanism and properties of a NI may depend not only on the numerical method and the nonlinear equation being simulated, but also on the simulated solution. This may raise a question as to why one even wants to study NI of a particular solution if NI of any other solution may be different? We propose the following answer. First, our emphasis is on understanding the *mechanism* of the NI, i.e. what makes certain modes go unstable. The number of such mechanisms is likely to be (much) smaller than the number of various solutions of various nonlinear equations. Having collected a "library" of such mechanisms, one can then identify one for a problem where one observes an NI. Second, it may be reasonable to expect that mechanisms and properties of NI of solutions that are, in some sense, similar to one another, can also be similar. (We will explain below why solitons (1.4) with $S = 0$ and $S = O(1)$ are *not* similar as far as *numerical* instability is concerned.) In Part III of this study we will demonstrate that oscillating solutions of the NLS or of its generalized version that includes a potential term, have the NI mechanism that is the same or very similar to that of the standing soliton [1]. Yet, some properties of the NI considered in Part III will be different from those in [1].

To conclude, let us comment on two issues. The first is the NI threshold for a moving soliton. From estimate (5.7a), one may conclude that such a threshold does not exist. This is because for arbitrarily small Δt (or, equivalently, C), there are always bands of wavenumbers k where $|R| > 1$ and hence the NI growth rate $\lambda > 0$; see (5.7b), (3.13), and (4.3). Thus, by the above argument, the FD-SSM would be unconditionally unstable. A more general (i.e. independent of the specifics of the model) justification of this conclusion can be based on (4.1). The operator on the r.h.s. of this eigenvalue problem and σ_3 on the l.h.s. are Hermitian. If the operator on the r.h.s. had been sign definite, $i\lambda$ would have been guaranteed to be real [7]; no NI would occur in this case. If one treats $i\partial_z$ as a *continuous* operator, it is sign indefinite and unbounded, and so the operator on the r.h.s. of (4.1) is sign indefinite for any μ (or C). Hence one cannot guarantee that $i\lambda$ is real; i.e., NI may (and generically will) occur. On the other hand, note that $i\partial_z$ is defined on the *discrete* grid and so it can only take on values within the interval $[-k_{\max}, k_{\max}]$. The sign indefiniteness of the entire operator on the r.h.s. of (4.1) may be caused by positive values of that operator. It is, however, eliminated once

one allows $\mu > Sk_{\max}$ (Here and below we neglect terms $O(1)$, keeping in mind that $k_{\max} \gg 1$ and $\mu \propto 1/C \gg 1$.) Using (4.1), where we approximate $\sin(K_0\Delta x/2) \approx 1$, and (2.2), we obtain the following order-of-magnitude estimate for the NI threshold:

$$\Delta t_{\text{thresh}} = \frac{1}{\sqrt{\pi|\beta|S}}\,\Delta x^{3/2}. \tag{6.1}$$

However, such an estimate is of no practical value. Indeed, we have repeatedly mentioned that our analysis had overestimated the NI growth rate, and already for $C = 0.7$ (and $K_{\text{sol}} \approx 1$), the NI may take $t > 1000$ to become just barely visible above the noise floor. For $C = 0.5$, it takes several thousand time units to appear above the noise floor, and for a yet smaller C it will take even longer. Thus, it is unlikely that such a weak NI could be significant in simulations.

The second issue is an explanation of why, in general, the NIs for the standing and moving solitons are different. More specifically, why does the NI of the standing soliton not occur, in the moving reference frame, for a moving soliton? Answers to both questions are based on the dispersion characteristic of the FD-SSM, shown in Fig. 2. For the general question, it suffices to note that the Galilean invariance of the NLS, manifested by the continuous parametrization of (1.4) by S, hinges on the dispersion characteristic of the NLS being quadratic (as shown in Fig. 2 for the Fourier SSM). Clearly, for high wavenumbers, where the NI occurs, the dispersion characteristic of the FD-SSM is not quadratic. Hence there is no reason to expect that the NIs of solitons with different S must be related.

To answer the specific question above, let us start by noting two facts. First, as we showed in Secs. 3 and 4 (see also [5]), NI occurs via interaction of *two* groups of Fourier harmonics (p- and q-terms in (3.7)). Second, if an unstable mode were to propagate along with the soliton, it would have to have the same group velocity as the soliton. Now, note that on the dispersion curve of the FD-SSM, there are only *two* points where the slope (i.e., the group velocity) has the same value $S = O(1)$. One of these two points — the closer one to $k = 0$ — corresponds to the moving soliton. The other point corresponds to one group (say, the p-term in (3.7)) of potentially unstable Fourier harmonics. But, there can be *no* third point with the same slope, which would have been required for the q-term to exists, and hence an interacting (p, q)-pair, leading to a NI, cannot occur. Note that for the standing soliton ($S = 0$), there are *three* locations on the dispersion curve where the slope is (almost) zero: at $k = 0$ and near $k = \pm k_{\max}$.

Acknowledgement

This research was supported in part by NSF grants ECCS-0925706 and DMS-1217006.

References

[1] T.I. Lakoba, Instability of the finite-difference split-step method applied to the nonlinear Schrödinger equation. Part I: Standing soliton, submitted.

[2] U. Ascher, Surprising computations, Appl. Numer. Math. 62 (2012), 1276–1288.

[3] J.A.C. Weideman and B.M. Herbst, Split-step methods for the solution of the nonlinear Schrödinger equation, SIAM J. Numer. Anal. 23 (1986), 485–507.

[4] T.I. Lakoba, Instability analysis of the split-step Fourier method on the background of a soliton of the nonlinear Schrödinger equation, Num. Meth. Part. Diff. Eqs. 28 (2012), 641–669.

[5] T.I. Lakoba, Instability of the split-step method for a signal with nonzero central frequency, J. Opt. Soc. Am. B 30 (2013), 3260–3271.

[6] M. Khanamiryan, O. Nevanlinna, and T. Vesanen, Long-term behavior of the numerical solution of the cubic non-linear Schrödinger equation using Strang splitting method, preprint, 2012; http://www.damtp.cam.ac.uk/user/na/people/Marianna/papers/NLS.pdf .

[7] I.M. Gelfand, *Lectures on linear algebra* (Interscience Publishers, New York, 1961), Sec. 15.